THE USE OF ESA STARMAPPER MEASUREMENTS FOR SPACECRAFT ATTITUDE ESTIMATION: ESTIMATOR DESIGN RATIONALE AND RESULTS

P.Th.L.M. van Woerkom F.J. Sonnenschein G. Moek

National Aerospace Laboratory NLR
Anthony Fokkerweg 2, Amsterdam, The Netherlands

ABSTRACT

In order to obtain highly accurate estimates of the attitude motion of spin-stabilized spacecraft one may decide to use a starmapper as basic attitude sensor. This reliable and versatile sensor detects the times of crossing of stars over photosensitive slits. Suitable data processing techniques are needed to transform the highly accurate measurements to highly accurate attitude estimates.
A prototype starmapper with Silicon detectors was built for ESA by the Institute of Applied Physics (TNO-TH, Delft). The National Aerospace Laboratory NLR has developed two computer programs for processing of ESA starmapper measurements.
This paper reviews the rationale followed in the design of the algorithms. Some numerical results produced by both programs are also presented, to illustrate their usefulness. Both programs are currently being developed towards operational use.

Keywords: Space vehicles, Satellite motion, Optical sensors, Star sensors, Attitude, Estimation, Filtering, Data processing.

1. INTRODUCTION

The attitude motion of spin-stabilized spacecraft can be estimated (reconstituted) by equipping the vehicle with suitable sensors. Some common examples of sensors used on spin-stabilized spacecraft are: Sun sensors, infra-red Earth sensors, magnetometers, and accelerometers.

As requirements on the accuracy of attitude estimation become more stringent, one observes a tendency to use star sensors as producers of attitude motion information. The very accurately known directions towards the detectable stars and the abundance of such stars all over the celestial sphere make star sensors attractive suppliers of attitude motion information. In addition, star sensors render attitude estimation accuracy independent of Sun/spacecraft/Earth collinearity, errors in apparent Sun or Earth diameter, distances to Sun or Earth, trajectory estimation errors, magnetic field modelling errors, and so on.

The principle of operation is as follows (Fig. 1). The star sensor consists basically of an optical system with straight photosensitive slits in its focal plane. The sensor is strapped down to the spacecraft, with the optical axis under a certain (cant-)angle with the intended spin axis. Due to the rotational motion of the spacecraft the sensor field of view scans a part of the celestial sphere. Stars passing through the field of view project images moving across the focal plane. The crossing of these images over the sensor slits is sensed by photo-detectors. If the signal thus generated is large enough to exceed an (adjustable) threshold level, then the time of crossing is registered, and telemetered to Earth, together (in general) with the identity of the slits involved.
Due to the scanning motion of the sensor field of view over the celestial sphere, the star sensor is usually known as "starmapper" or, equivalently, "starscanner" (Ref. 1).

The concept of equipping spin-stabilized spacecraft with starmappers acquired interest in the mid nineteen-sixties (Refs 2,3).
The earlier starmappers used one or more photo-multiplier tubes behind the slits.
The earlier attitude estimation techniques where typically simple geometrical techniques (no nutation), or more sophisticated least squares batch processing techniques (nutation and misalignments sometimes included) which used geometrical "measurements" derived from the actual time-measurements by some method of preprocessing.

A relatively recent and important improvement to the starmapper instrument has been the replacement of the photo-multiplier tube by solid state detectors. Starmappers with solid state detectors have, at present, a smaller signal-to-noise ratio. However, they have important advantages, such as size, increased ruggedness, stability, and spectral range, and low sensitivity to straylight, background noise, and overexposure (Ref. 4).
The Institute of Applied Physics (TNO-TH, Delft) designed, developed, and constructed a starmapper of this type for the European Space Agency ESA (Refs 4-6). There are eight slits in the focal plane, each integrated with its own Silicon detector and its own signal conditioning electronics. Great operational redundancy is achieved through the unique slit configuration chosen. The design can be optimized by tuning geometrical, optical, and electronic parameters to the given spacecraft configuration. The instrument can be used on spacecraft with spin rates up to about 50 rpm.

Coupling the use of such an advanced attitude sensor to the use of advanced attitude estimation

Proc. Int. Symp. Spacecraft Flight Dynamics, Darmstadt, FRG, 18-22 May 1981 (ESA SP-160, Aug. 1981)

algorithms raises the prospect of accurate estimation of a variety of attitude- and attitude related parameters (attitude angles, angular velocities, moments of inertia, misalignments, external disturbance torques, ...).
To investigate the possibilities for realizing this prospect the European Space Agency requested the National Aerospace Laboratory NLR (Amsterdam) to formulate several attitude estimation algorithms, to implement these on the general purpose digital computer at NLR, and to carry out exploratory numerical simulations.
The present paper describes some of the many considerations underlying the design of the attitude estimation algorithms. Results from some numerical simulations are presented to illustrate their usefulness.

2. MODELLING SPACECRAFT ATTITUDE MOTION

Of prime interest is the evolution of the spacecraft attitude with respect to a given, inertially oriented, celestial reference frame $\{\bar{X}_C\}$.
It is assumed that the spacecraft attitude motion is represented accurately by that of single spin, rigid body motion. Furthermore, the half-cone nutation angle is assumed to be of the order of several degrees (at most).

Introduce a body fixed, principal axes reference frame $\{\bar{X}_B\}$. Both frames are related through the rotation matrix $T_{B,C}$,

$$\{\bar{X}_B(t)\} = T_{B,C}(\bar{\alpha},\bar{\varphi}(t)\ \{\bar{X}_C\} \qquad (1)$$

The vector $\bar{\varphi} \triangleq (\varphi_1,\varphi_2,\varphi_3)^T$ defines the time-varying attitude motion with respect to an intermediate, inertially oriented reference frame $\{\bar{X}_L\}$. The constant vector $\bar{\alpha} \triangleq (\alpha_1,\alpha_2)^T$ defines the orientation of frame $\{\bar{X}_L\}$ with respect to frame $\{\bar{X}_C\}$.
The purpose of frame $\{\bar{X}_L\}$ depends on the nature of the estimation algorithm under consideration. For example, one may use $\{\bar{X}_L\}$ to define the time-averaged orientation of the spin axis (as is done, e.g., in Section 5.1). Or, one may use $\{\bar{X}_L\}$ to allow linearization of the kinematic equations (as is done, e.g., in Section 5.2). In short, $\{\bar{X}_L\}$ is introduced for mathematical convenience.

The dynamic (Euler) and kinematic equations can now be written out, to yield

$$\dot{\bar{x}} = \bar{f}(\bar{x},\bar{\lambda},\bar{M}/I_{Z_B}) \qquad (2)$$

where $\bar{x} \triangleq (\bar{\varphi}^T,\bar{\omega}^T)^T$, and $\bar{\omega}$ is the spacecraft angular velocity vector. The vector $\bar{\lambda} \triangleq (\lambda_1,\lambda_2)^T$ is the moment-of-inertia-ratio vector, based on the moments of inertia of the spacecraft, with

$$\lambda_1 \triangleq (I_{Z_B}-I_{X_B})/I_{X_B},\quad \lambda_2 \triangleq (I_{Z_B}-I_{Y_B})/I_{Y_B} \qquad (3)$$

Specifically, I_{Z_B} is the spacecraft moment of inertia with respect to the intended spin axis Z_B. The vector $\bar{M} = \bar{M}(\bar{x},t)$ represents the total torque exerted on the spacecraft.
In this paper the known deterministic part of $\bar{M}$ (effective thruster torques, environmental torques, ..) is neglected, for the sake of simplicity. Inclusion of the known deterministic part of $\bar{M}$ is straightforward in principle.
The unknown deterministic and the stochastic part of $\bar{M}$ may be modelled as piecewise linear functions of time,

$$\bar{m}(t) = \bar{m}(t_k) + (t-t_k)\bar{\xi}_k \quad , \quad (t_k<t<t_{k+1}) \qquad (4)$$

where $\bar{m} \triangleq \bar{M}/I_{Z_B}$, $\bar{\xi}_k$ represents a Gaussian white noise sequence, and t_k represents the time of measurement. Note the possibility of a jump in the slope of $\bar{m}(t)$ at each time of measurement.

The dynamic (Euler-) equations in (2) may be linearized in the presence of moderate to small nutation and small external torques. The kinematic equations in (2) may be linearized by suitable choice of the intermediate, linearization reference frame $\{\bar{X}_L\}$; i.e., by suitable choice of $\bar{\alpha}$. The result is that (2) can be integrated analytically, to yield the compact recursive solution (Refs 7 and 11)

$$\bar{x}_k = \bar{f}(x_{k-1},\bar{m}_{k-1},\bar{\lambda},t_k-t_{k-1}) + \bar{\omega}_k \qquad (5)$$

The term $\bar{\omega}_k$ represents linearization errors, the random torque-slope variable $\bar{\xi}_k$, and effects of remaining modelling errors.
Note that the three moments of inertia appear only through the two moment-of-inertia ratios λ_1,λ_2. Note also that the spacecraft mass distribution may be asymmetric ($\lambda_1 \neq \lambda_2$).

Care must be exerted in the choice of attitude parameters. In the present study the attitude vector $\bar{\varphi}$ represents the Tait-Bryan (1-2-3) angles. Advantages of the use of these angles, rather than the classical Euler angles, are that the attitude parametrization is singularity-free in the present case of moderate to small nutation angles (specifically in the desirable limit of zero nutation), and that it facilitates visualization of the evolution of the attitude, even for relatively arbitrary $\bar{\lambda}$ and $M(\bar{x},t)$ (see Refs 7 and 11).

3. MODELLING THE STARMAPPER

Define a detector reference frame $\{\bar{X}_D\}$ with origin in the optical center of the starmapper, with Z_D axis normal to the detector plane, and with X_D axis in the plane through Z_D and the nominal (or intended) spin axis Z_B (Fig. 2). Again considering orientations only, one has

$$\{\bar{X}_D\} = T_{D,BN}(\bar{\beta})\ \{\bar{X}_{BN}\} \qquad (6)$$

where $\bar{\beta} \triangleq (\beta_1,\beta_2)^T$ defines the nominal azimuth β_1 and the nominal cantangle β_2 of the starmapper in $\{\bar{X}_{BN}\}$. The frame $\{\bar{X}_{BN}\}$ coincides with the body fixed, principal axes reference frame $\{\bar{X}_B\}$ under nominal conditions.
Shifts in spacecraft mass distribution and instrument misalignments result in a different orientation of frame $\{\bar{X}_D\}$ with respect to $\{\bar{X}_B\}$,

$$\{\bar{X}_D\} = T_{D,B}\ \{\bar{X}_B\} \qquad (7)$$

where the rotation matrix $T_{D,B}$ is a function of $\bar{\beta}$ and of the above-mentioned mass shifts and instrument misalignments.
Expressions (6) and (7) can be interpreted by visualizing $\{\bar{X}_{BN}\}$ as a new frame that is immutably oriented with respect to $\{\bar{X}_D\}$, through $\bar{\beta}$. Then, the effect of mass shifts and instrument misalignments is to rotate this new, intermediate frame $\{\bar{X}_{BN}\}$ with respect to $\{\bar{X}_B\}$.
More specifically, let the orientation of $\{\bar{X}_{BN}\}$ with respect to $\{\bar{X}_B\}$ be parametrized by the three successive rotation angles $\gamma_1 \rightarrow \gamma_2 \rightarrow \gamma_3$ in figure 3.

For small mass shifts and small misalignments one has $|\gamma_2|,|\gamma_3|<<1$, and arbitrary γ_1. It turns out that equation (7) can be rewritten as

$$\{\bar{X}_D\} = T_{D,BN}(\bar{\beta})\ T_{BN,B}(\bar{\gamma})\ \{\bar{X}_B\} \qquad (8)$$

Comparison of (8) with (6) and (7) then shows that the angles γ_1, γ_2 and γ_3 can be interpreted as "effective" misalignment angles, which adequately represent the combined effects of mass shifts and misalignments on the overall rotation matrix $T_{D,B}$.

Having defined the orientation of the detector frame $\{\bar{X}_D\}$ with respect to the actual principal axes frame $\{\bar{X}_B\}$ (Eq. (8)), and the orientation of $\{\bar{X}_B\}$ with respect to the celestial frame $\{\bar{X}_C\}$ (Eq. (1)), it becomes possible to relate the direction to a star in $\{\bar{X}_C\}$ to the associated direction to that star in $\{\bar{X}_D\}$.
Let the unit vector $\bar{u}$ to the star under consideration be known as $\bar{u}_C$ in frame $\{\bar{X}_C\}$. From (1) and (8) one finds for the same unit vector in frame $\{\bar{X}_D\}$,

$$\bar{u}_D = T_{D,BN}(\bar{\beta})\ T_{BN,B}(\bar{\gamma})\ T_{B,C}(\bar{\alpha},\bar{\varphi}(t))\bar{u}_C \qquad (9)$$

The light of that star is projected on the detector plane at focal distance from the lens (Fig. 4). The detector plane reference frame $\{\bar{X}_{DP}\}$ parametrizes the detector plane. The location of the star image then follows from

$$\bar{\rho}_{DP} = -F_o\ \bar{h}(\bar{u}_D) \qquad (10)$$

where F_o represents the focal length of the optics, and where $\bar{h}$ is a nonlinear operator which defines the projection of the star onto the planar frame $\{\bar{X}_{DP}\}$, and accounts for optical distortion.

The location of the slits in the detector plane is accurately described in the pattern reference frame $\{\bar{X}_P\}$ (Figs 5,6). In the case of the ESA starmapper (Refs 3-5) there are eight independent slits, four of which are parallel to the X_P axis, and four of which are under 45 degrees with respect to the X_P axis (Fig. 6). The location of the star image in $\{\bar{X}_P\}$ then follows from

$$\bar{\rho}_P = -\begin{pmatrix}\delta_1\\ \delta_2\end{pmatrix} + \begin{pmatrix}1 & \delta_3\\ -\delta_3 & 1\end{pmatrix}\bar{\rho}_{DP} \qquad (11)$$

where the vector $\bar{\delta} \triangleq (\delta_1,\delta_2,\delta_3)^T$ defines small translational and rotational misalignments between $\{\bar{X}_{DP}\}$ and $\{\bar{X}_P\}$ (Fig. 5).

A measurement is made whenever the image of a star crosses one of the slits; in other words, whenever the tip of the image vector $\bar{\rho}_P$ crosses one of the slits. The occurrence of such a crossing is called a "geometric event"; the associated time of crossing is called a "geometric time of crossing".
One may now write the functional relationship

$$\bar{\rho}_P(t) = \bar{\rho}\{\bar{\alpha},\bar{x}(\bar{m},\bar{\lambda},t),\bar{\beta},\bar{\gamma},\bar{\delta},\bar{u}_C\} \qquad (12)$$

Define the geometry of slit j (j= 1,2,..,8) in the $\{\bar{X}_P\}$ frame by $f^{(j)}(X_P,Y_P)= 0$. Note that the slit need not be straight, and need not pass through the origin. The measurement equation now reads:

$$f^{(j)}\{X_P(t_k),Y_P(t_k)\} = 0 \qquad (13)$$

where t_k is the geometric time of crossing of the image (projection) of the star over slit j.

The times of crossing as telemetered to Earth are called "actual measurements". They differ from the geometric times of crossing. Differences are generated, e.g., by optical point-spreading, electronic delays, electronic noise, onboard clock resolution, and telemetry resolution.
Let the actual measurement be denoted by $t_{m,k}$ and let again the geometrical crossing time be t_k. Thus, one has a measurement error $\delta t_k \triangleq t_{m,k} - t_k$. Analysis of the measurement error sequence δt_k(k= 1,2,...) produced by the truth model of the starmapper instrument shows that δt_k is composed of a virtually constant part (actually, a rather insensitive function of starmagnitude and temperature) and a random part (zero mean, white noise sequence). By correcting the actual measurements for the known or estimated constant part of δt_k, the remaining measurement errors in δt_k will form a zero mean, white noise sequence.

Remark: In literature one usually encounters a measurement equation of a different type. Define $S^{(j)}$ as the plane through the straight slit j and the optical center of the starmapper. Let $\bar{n}_D^{(j)}$ be the unit normal to $S^{(j)}$, expressed in $\{\bar{X}_D\}$. The measurement equation for slit j then reads

$$\bar{n}_D^{(j)}\ .\ \bar{u}_D(t_i) = 0 \qquad (14)$$

Disadvantages of this method are that the slits must be straight and that optical nonlinearity must be negligible. Also, the measurement error defined by (14) possesses statistics that depend on the parameters one seeks to estimate (state dependent measurement noise). Indeed, the measurement error follows from (14) as

$$\delta_k \triangleq \{\bar{n}_D^{(j)}\}^T\ \bar{u}_D(t_{m,k}) - \{n_D^{(j)}\}^T\ \bar{u}_D(t_k)$$
$$\cong \{\bar{n}_D^{(j)}\}^T \left\{\frac{\partial u_D}{\partial \bar{x}}\ \frac{d\bar{x}}{dt}\right\}_{t_{m,k}}\ \delta t_k$$

Whereas the statistics of δt_k do not depend on $\bar{x}(t)$ (at least to the lowest order), this desirable property is seen not to hold anymore for δ_k. Therefore, use of (14) would complicate the design of a statistically optimized estimator.

4. PARAMETERS TO BE ESTIMATED

Reviewing equations (12) and (13) one has the following categories of measurement-defining vectors:
- known vector:
  - $\bar{\beta}$ (nominal starmapper orientation)
- generally unknown vectors:
  - $\bar{x}$ (containing attitude vector $\bar{\varphi}$ and angular velocity vector $\bar{\omega}$)
  - $\bar{m}$ (stochastic external torque vector)
  - $\bar{\lambda}$ (moment-of-inertia-ratio vector)
  - $\bar{\gamma}$ (effective reference frame misalignment vector)
  - $\bar{\delta}$ (slit misalignment vector)
- vectors that are sometimes known, sometimes unknown (see Sections 2 and 5):
  - $\bar{\alpha}$ (orientation of intermediate frame $\{\bar{X}_L\}$)
  - $\bar{u}_C$ (unit vector towards crossing star).

As mentioned before, the incorporation of deterministic external torques is not discussed in the present paper.

There exists a trade-off between the transverse angular velocities ω_{XB} and ω_{YB}, and the two intermediate angles α_1 and α_2.

For example, in the application in Section 5.1 one estimates α_1 and α_2 under the constraint $\omega_{XB} \doteq 0$, $\omega_{YB} \doteq 0$, whereas in the application in Section 5.2 one specifies α_1 and α_2, but estimates ω_{XB} and ω_{YB} (in addition to many other unknowns). Before one has identified the star that produces a given measurement, the vector $\bar{u}_C$ is unknown. Vector $\bar{u}_C$ is known only upon identification of the star(s).

5. CHOICE OF ESTIMATION ALGORITHM

Choosing a suitable algorithm for the estimation of some or all of the unknown parameters listed in Section 4 involves the analysis of a variety of trade-offs. These trade-offs are related to: choice of the parameters to be estimated, modelling errors that may be present, on- or off-line processing, the problem of star-identification, number of measurements available, parameter observability, spacecraft maneuver requirements, abundance of spurious measurements ("false events") and of measurements produced by uncatalogued stars, total timespan of measurement collecting, and so on.
To keep this paper limited in size, a sketch will be given of some of the reasons that led to the formulation and implementation of two estimation algorithms for use in ground based computers. Section 6 describes some numerical results produced by these two algorithms, with measurements obtained from mathematical truth models of sky, spacecraft, and starmapper (Fig. 7).
Whatever algorithm is used, one must have available a "sky model", containing the directions to stars, sun, and other bright celestial bodies as seen from the spacecraft, as well as (at least approximate) information on the brightness of the stars. This skymodel is needed to identify the stars whose slitcrossings are detected, and to determine the attitude of the spacecraft with respect to that skymodel.
The brightness indicated should be the detector brightness; i.e., the brightness of the stars as perceived by the (Silicon-) photo-detectors.

5.1 Batch processor for the acquisition of an attitude estimate

The batch processor is a very robust computer program based upon simplified spacecraft- and starmapper models. It is used for quick-look purposes, as well as for the production of rough initial attitude estimates required as input into the more sophisticated recursive processor to be described below (Sect. 5.2, and Fig. 7).
The program can be used in the absence of any a priori estimate about the attitude motion of the spacecraft. For additional robustness and reduction in data processing effort it is assumed that a Sun sensor is available. This Sun sensor is assumed to be of the V-slit type (one vertical and one inclined slit); however, a digital solar aspect sensor would provide equivalent information. Only some (any) combination of two or four out of the total of eight independent starmapper slits is used, such, that a V-configuration is formed in $\{\bar{X}_P\}$ (examples: slits 1-2, or slits 1-3-7-8, and so on; see Fig. 6).
The starmapper trigger level (essentially a star-brightness discrimination level) can be adjusted to facilitate star identification (too many or too few measurements per revolution make star identification difficult). Trigger level adjustment is to be executed by the ground controller.
Some details are sketched below; see also references 8 and 9.

The spacecraft is modelled as a pure spinner. This implies $\omega_{XB} \equiv \omega_{YB} \equiv 0$. Also, $\omega_{ZB} \doteq$ constant. Consequently, the inertia ratio vector $\bar{\lambda}$ becomes unobservable. The misalignment vectors $\bar{\gamma}$ and $\bar{\delta}$ are set zero. Let the angles α_1, α_2 define the orientation of the spacecraft intended spin axis in $\{\bar{X}_C\}$. Thus, defining $\varphi_3(o)$ as the spacecraft phase angle at t= 0, one finds that $\varphi_1 \equiv \varphi_2 \equiv 0$. In conclusion, four parameters are estimated:
- angular coordinates $\bar{\alpha}$ of the spin axis in $\{\bar{X}_C\}$
- phase angle at initial time, $\varphi_3(o)$
- spin rate, ω_z.

Briefly, the algorithm contains the following elements (Fig. 8):
- spacecraft spin rate is estimated by processing the times of solar crossings of the vertical Sun-sensor slit;
- to reduce the sensitivity of the measurements to non-negligible nutation, external torques, false sensor events, detection probabilities, and sensor and telemetry random errors, the telemetered crossing times are averaged after correction for the estimated spin period (as determined above). The result is a set of average crossing times of as yet unidentified stars over the operational slits of the starmapper, and of the Sun over the slits of the Sun sensor. These average times are called "repeatable events";
- having established the repeatable events of the celestial bodies (Sun and stars) for the various operational slits, one now determines which of the repeatable events on adjacent slits have been produced by the same celestial body. With the Sun sensor, correlation is trivial. With the starmapper, one compares the time intervals between repeatable events at adjacent slits;
- given the repeatable events produced by the same celestial body at adjacent sensor slits, one uses simple spherical trigonometry to derive elevation and relative azimuth (with respect to an as yet unknown reference direction) of that celestial body in an inertially despun spacecraft reference frame (using a simplified version of Eq. (12));
- given the "observed sky model" just constructed, one attempts to identify the repeatedly observed celestial bodies by fitting this model to the "reference sky model", the latter containing the directions to stars, Sun, Earth and Moon with respect to the celestial reference frame $\{\bar{X}_C\}$. The result of this identification procedure, based on matching of the cosines of the angular separations between celestial bodies in triplet configurations, is that one knows the direction to each of the observed and subsequently identified celestial bodies both in the despun spacecraft reference frame and in the celestial reference frame used in the reference sky model;
- given the directions to observed and subsequently identified celestial bodies, both in the despun reference frame and in the celestial reference frame, one can unambiguously determine the attitude of the spacecraft (α_1, α_2) and the initial phase angle ($\varphi_3(o)$).

Details can be found in reference 9. Recall that a priori estimates of the attitude are not required at all, and that the output consists of

the averaged orientation of the spin axes, the averaged initial spacecraft phase angle, and the averaged spin rate (therefore constants). This output is sufficient for quick-look purposes. If more refined estimates are required, and if estimates of other parameters (nutation, misalignments, inertia ratios ...) are required as well, then one uses the output thus obtained as input into the recursive processor to be described below (Fig. 7).

5.2 Recursive processor for fine estimation

The recursive processor is a computer program which uses detailed spacecraft- and starmapper models (basically those sketched in Sections 2 and 3), and which processes the starmapper measurements one at a time.
The parameters to be estimated are those listed under "generally unknown vectors" in Section 4. However, it is possible to treat certain parameters as consider parameters; that is to say, the numerical values of those parameters are acknowledged to be in error (uncertainty), but these values are not updated. This procedure enhances -at times- estimation stability.

Loosely speaking, the fine estimation algorithm used is the discrete extended Kalman estimation algorithm. Defining the state vector $\bar{z} \triangleq (\bar{\varphi}^T, \bar{\omega}^T, \bar{m}^T, \bar{\lambda}^T, \bar{\gamma}^T, \bar{\delta}^T)^T$ (see Section 4), the Kalman filter uses the spacecraft- and starmapper models discussed before, together with the incoming starmapper measurements, to provide a minimum variance estimate $\hat{\bar{z}}_k$ of the actual state vector $\bar{z}_k$ associated with each measurement time t_k. The mathematical models used in the fine estimation algorithm account for nonzero nutation, for unknown and possibly asymmetric spacecraft mass distribution, for a variety of misalignments, and for random torques with nonzero mean.
The recursive nature of the algorithm has several advantages: computational requirements are modest, since the measurements are processed one by one (an important advantage, even with the-present-use of ground-based computers); on-line estimation becomes possible; estimates of the statistical quality (standard deviation) associated with the parameter estimates $\hat{\bar{z}}_k$ are generated on-line; parameter observability tests are relatively straightforward; time-variations in system- and measurement noise are accommodated easily; spacecraft maneuvers can be accommodated easily; confidence in the a priori estimates (i.e., a priori covariance matrix) can be introduced directly; and, quite important: parameters modelled as constants (such as misalignments, and, indirectly, spin rate, angular momentum vector and nutation angle) can in reality be time-varying with the algorithm still tracking their actual, current values (example: unmodelled spin rate variations).

However, two aspects requiring special care must be mentioned.
First, the a priori estimate $\hat{\bar{z}}_o$ at initial time t_o must be of sufficient accuracy. In the present case this a priori estimate is to be provided by the batch processor described above (Section 5.1 and Fig. 7). The availability of $\hat{\bar{z}}_o$ can subsequently be exploited for substantial reduction of the sky model used by the recursive processor, since one now needs a sky model containing only those stars that are located in the expected swath on the celestial sphere (Fig. 1).

Second, there is the problem of sensitivity to modelling errors. The mathematical models used in the algorithms must be fairly accurate. Otherwise, filter divergence may occur, implying more or less serious reduction in reliability of the estimates produced by the algorithm. In the present case sensitivity to modelling errors is monitored and subsequently (but on-line) abated through introduction of a certain filter divergence detection and adaptation technique; see below.

The basic steps in the fine estimation algorithm are the following (Fig. 9):
- let t_k be the measured time of crossing of a star over a given slit;
- using the most recent, available estimate (associated with time t_{k-1}), calculate the predicted time of crossing $\tilde{t}_k$ with associated predicted state $\tilde{\bar{z}}_k$ and covariance matrix $\tilde{\Lambda}_k$;
- calculate the optimal update gain K_k;
- calculate the measurement residual and carry out the update, yielding $\hat{\bar{z}}_k$ and covariance matrix $\hat{\Lambda}_k$ at time t_k;
- accept the next measurement t_{k+1} and repeat the above cycle.

Actually, the algorithm is more involved. For example:
- star identification is carried out, using measurement residuals (a crossing-time matching technique, in which measured times are compared with predicted times;
- to account for model nonlinearities the algorithm is written in the "extended iterated" form;
- numerical stability is improved by propagating the covariance matrix Λ in square root form;
- the measurement residuals are monitored to test for proper operation of the estimator, and a sensitive, nonlinear algorithm is used for on-line detection of filter divergence;

In the present case of spacecraft attitude reconstitution filter divergence is interpreted as resulting from unmodelled perturbing torques acting on the spacecraft. These torques may be described as pure random torques, or, more refined, as low-order polynomials in time between any two successive measurement times plus a random component (e.g., Eq. (4)). In the latter case the coefficients of the polynomials are estimated as well.
The predicted covariance matrix $\tilde{\Lambda}_k$ is now adjusted as a function of the influence of the hypothesized, divergence inducing torques on the spacecraft attitude motion, and as a function of the intensity of the filter divergence. The direct result is that the new measurement is weighted more heavily (adaptation).

More details can be found in references 10 and 11. A description of the technique of divergence detection and subsequent adaptation of the type used in the present study can also be found in the seminal paper under reference 12.

5.3 Comment

Recall that the batch processing algorithm described in Section 5.1 is based on the use of simplified spacecraft- and starmapper models. The output describes the averaged orientation of the spin axis, the averaged initial spin phase angle, and the averaged spin rate; thus, four

constants in total.
Of course, the batch processing algorithm could have been based on more sophisticated spacecraft- and starmapper models. This was not done, however, since the purpose of the study reported in Section 5.1 was only to obtain a robust and simple algorithm to produce initial conditions for the more advanced recursive processing algorithm described in Section 5.2 (Fig. 7).

The recursive processing algorithm described in Section 5.2 is based on more sophisticated spacecraft- and starmapper models. Normally, output consists of estimates of $\bar{\varphi}_k$, $\bar{\omega}_k$, $\bar{\lambda}$, $\bar{\gamma}$, and $\bar{\delta}$. However, the algorithm allows estimation of time-varying external torques as well (vector $\bar{m}_k$). The output then consists of seventeen quantities, nine of which are modelled as generally time-varying ($\bar{\varphi}_k$, $\bar{\omega}_k$, $\bar{m}_k$). Due to the recursive nature of the algorithm it is nevertheless possible to track slow-time-variations in the remaining eight "constants" as well (examples: time-varying misalignments, and time-varying moments of inertia). Thus, the term "fine estimation" is used in the title of Section 5.2 for the simple reason that the many parameters estimated through this algorithm yield deeper insight into the behavior of the "fine structure" of the spacecraft/starmapper system.

6. SOME NUMERICAL RESULTS

Some numerical results obtained with each of the two algorithms are briefly presented below. They are only meant to illustrate the usefulness of the algorithms. They are not necessarily indicative of the ultimate estimation accuracy that might be achieved under given circumstances.

The (pseudo-) measurements generated by the truth models were based on (amongst others) the following data: spin rate 10 rpm, inertia ratios $\lambda_1 = \lambda_2 = 0.1$, no misalignments, no external torques, starmapper cantangle $\beta_2 = 30^\circ$, starmapper field of view $7.9^\circ \times 7.9^\circ$, no active telemetry constraints, data collection during 60 seconds (one nutation period).

6.1 Batch processor

In this first numerical example the operational starmapper slits are numbers 3-4-5-7 (Fig. 6), the inclined sun sensor slit makes an angle of 30° with the vertical slit, and the true (half-cone) nutation angle is 15 arcminutes.
One finds that four stars (Fig. 10) produce events that are "repeatable" and that can be correlated. Taking into account the Sun it is possible to identify these stars from a sky model containing 177 candidate stars. The (averaged) attitude motion parameters are reconstituted with the following true errors: spin period error = 5×10^{-5}s or 8.3×10^{-4} %, and error in the averaged attitude (i.e., in the angular momentum vector) = 58 arcsec. A large number of simulations has shown that the batch processor developed by NLR is remarkably robust with respect to a large variety of spacecraft-, sun sensor-, and starmapper alignment errors.

6.2 Recursive processor

The recursive processor does not use sun sensor measurements. In both examples to be presented all starmapper slits are operational, and the true (half-cone) nutation angle is 30 arcminutes. The orientation of the angular momentum vector in the two examples differs from the one simulated in Section 6.1. Three stars are detected, and repeatedly identified with the aid of a reduced sky model containing 5 candidate stars only.

In the first example to be presented here, all misalignments and moment-of-inertia ratios are assumed to be well-known (near-zero a priori uncertainty). Estimator performance is illustrated in figures 11-14. Figure 11 displays the divergence detection parameter y. Proper estimator operation is indicated by $0 \leq y \leq 0.15$. Apparently, at times there is a tendency towards divergence (indicated by $y > 0.15$), which is subsequently suppressed successfully by the adaptation mechanism. Figures 12 and 13 show the true error in the estimates of phase angle φ_3 and one of the transverse attitude angles, φ_1, as well as their estimated standard deviations. Note that the estimation errors in φ_3 and φ_1 are fractions of an arcminute only. The true and estimated nutation angles are shown in figure 14.

The second numerical example is shown in figures 15-20. The difference with the first example is that now much larger a priori errors and associated uncertainties are attributed to the various misalignments (0.1° in both γ_2 and γ_3) and moment-of-inertia ratios (10 % in both λ_1 and λ_2). Since the available measurements are now used to substantially reduce the (larger) a priori errors and uncertainties of many more parameters, one finds that the tendency towards divergence has increased somewhat (larger values of the divergence detection parameter y in Fig. 15). Since errors and uncertainties in misalignments in azimuth direction are to be reduced as well, the reduction in error and uncertainty in the phase angle φ_3 is somewhat less dramatic now (Fig. 16; compare with Fig. 12). A similar remark applies to the estimation of the transverse attitude angles (φ_1 in Fig. 17; compare with Fig. 13). At the same time the a priori uncertainty about the misalignments and the moment-of-inertia ratios is now decreased (e.g., γ_2 in Fig. 18, and λ_1 in Fig. 19). True and estimated nutation angles are shown in figure 20. (Remark: in other simulations it was found that the errors and uncertainties in attitude $\bar{\varphi}$ and in angular velocity $\bar{\omega}$ can be further reduced if the remaining parameters are not estimated anymore but instead are treated as "consider parameters").
The latter experience shows that the recursive estimator, together with the various truth models, can also be used as a valuable tool for trade-off analysis of required attitude reconstitution accuracy versus required instrument alignment accuracy.

7. CONCLUSIONS

An outline has been presented of the design rationale followed by the National Aerospace Laboratory NLR in the design of two attitude estimation algorithms to be used for processing measurements from the ESA starmapper. In order to test their proper functioning and to

investigate their usefulness, certain truth models for (pseudo-) measurement generation were developed as well.

The batch processor turned out to be quite robust with respect to a variety of errors. The true error in the (averaged) attitude estimate is typically of the order of one arcminute. It is useful to have an operator in the loop to adjust estimator tolerances and/or trigger levels whenever star identification is not immediately successful (due to too many or too few measurements per spin period).
Note that the batch processor operates very efficiently with measurements taken over one nutation period only (smaller time intervals are also possible). Considering the context of spinning spacecraft this amounts to (near-) online estimation.

The recursive processor uses the output from the batch processor as input. It uses a reduced sky model, monitors proper operation of the estimation process on-line, introduces statistical adaptation when necessary, and produces more detailed information on the attitude motion of the spacecraft, misalignments of the starmapper, spacecraft mass re-distribution, and external torques, whether time-varying on fast or slow time scale.

8. REFERENCES

1. Gutshall R L & Deters R A 1979, A survey of attitude sensors, J. Astronautical Sciences, XXVII (3), 217-238.

2. Grosch C B 1967, Orientation of a rigid torque-free body by use of star transits, J. Spacecraft & Rockets, 4(5), 562-566.

3. Walsh T M, Keating J C, & Hinton D E 1968, Attitude determination of the spin-stabilized Project Scanner spacecraft, NASA TN D-4740.

4. Hammerschlag A et al 1973, Design and development of a starmapper breadboard model Phase I, ESRO CR-162.

5. Boom C W de, Hammerschlag A, & Oprel P J 1977, Design and development of the Starmapper prototype Phase IV, ESA CR(P)-957.

6. Boom C W de 1977, Starmapper: a sensor for attitude determination of spinning spacecraft, Proc. of the AOCS Conference, Noordwijk, 3-6 October 1977, ESA SP-128, 303-308.

7. Woerkom P Th L M van 1975, Analysis of the perturbed motion of asymmetric, spinning spacecraft, National Aerospace Laboratory NLR, TR 75043 U.

8. Woerkom P Th L M van & Sonnenschein F J 1980, Spacecraft attitude measurement using the ESA starmapper, ESA Journal, 4(3), 287-294.

9. Woerkom P Th L M van & Sonnenschein F J 1980, Study of an attitude acquisition measurement technique using the ESA starmapper - Final report, ESA CR(P), to be issued.

10. Woerkom P Th L M van & Traas C R 1979, Accurate spacecraft attitude estimation with the ESA starmapper, Proc. 8th IFAC Symposium on Automatic Control in Space, Oxford 2-6 July 1979.

11. Woerkom P Th L M van, Traas C R, Bleekrode A L, Sonnenschein F J & Bokhove H 1978, Study of spacecraft attitude reconstitution with the ESA starmapper, ESA CR(P)-1192.

12. Traas C R 1976, Estimation of modelling errors in satellite attitude determination, National Aerospace Laboratory NLR, MP 76019 U (also: 1977, Acta Astronautica, 4(9-10), 1059-1073).

ACKNOWLEDGEMENT

This paper is based on work performed for the European Space Agency under ESTEC contracts 2383/75/AK and 3625/78/AK monitored by Dott. Ing. D. Sciacovelli, and under ESOC contract 4133/79/D/IM monitored by Dr. L. Fraiture. Mr. H. Bokhove (Institute of Applied Physics TNO-TH, which designed and developed the ESA starmapper), Dr. C.R. Traas (NLR, presently at the Twente University of Technology, Enschede), and Mr. A.L. Bleekrode (NLR) participated in the earlier part of the contract work.

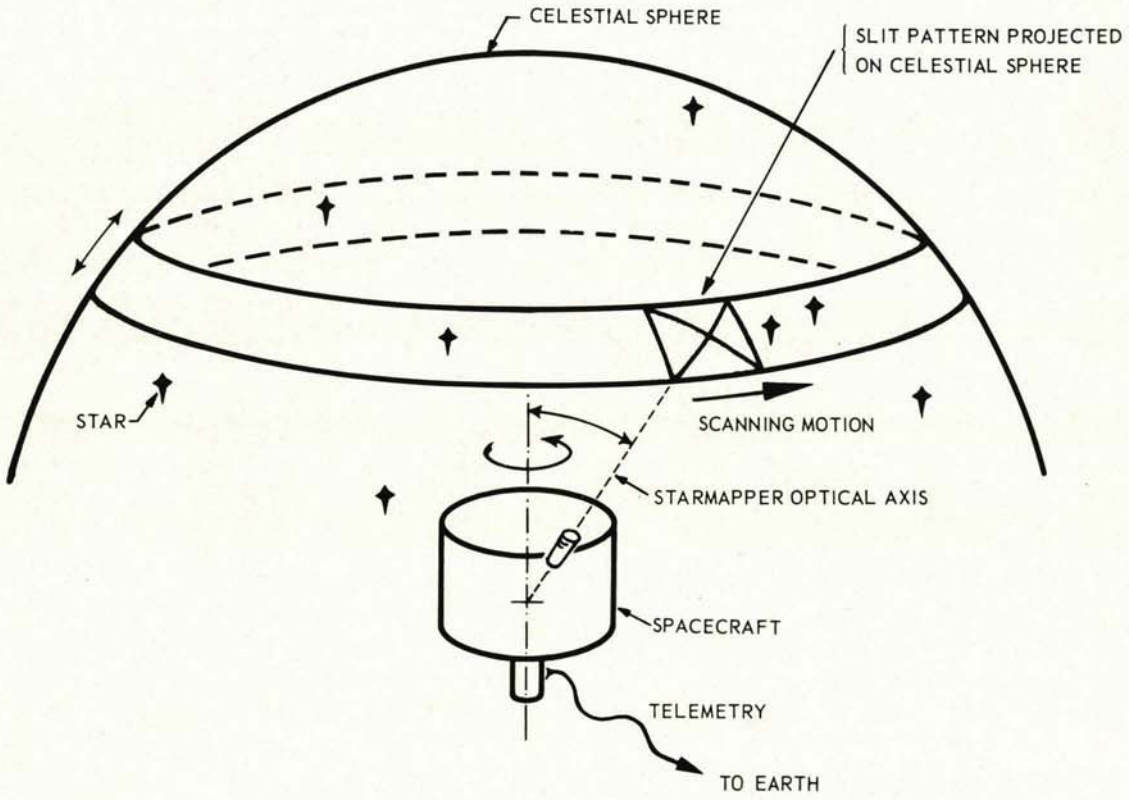

Figure 1. Principle of starmapper operation (sketch). The figure shows the projection of the sensor slits as it moves over the celestial sphere.

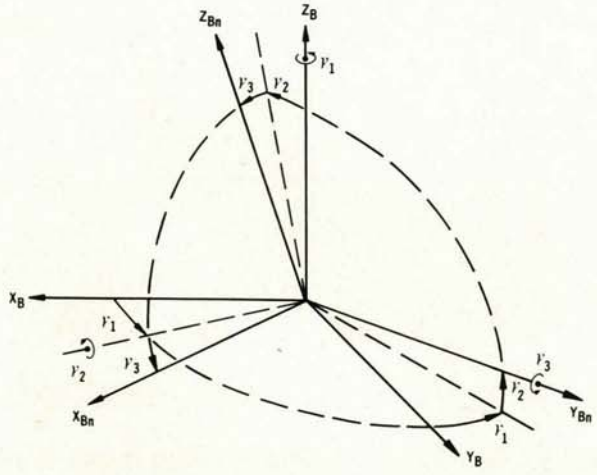

Figure 2. Nominal body reference frame $\{\bar{X}_{BN}\}$ and detector reference frame $\{\bar{X}_D\}$. Note that $\{\bar{X}_D\}$ axes are parallel to $\{\bar{X}_D^*\}$ axes. Angle β_1 is nominal azimuth of optical axis Z_D; angle β_2 is nominal cantangle.

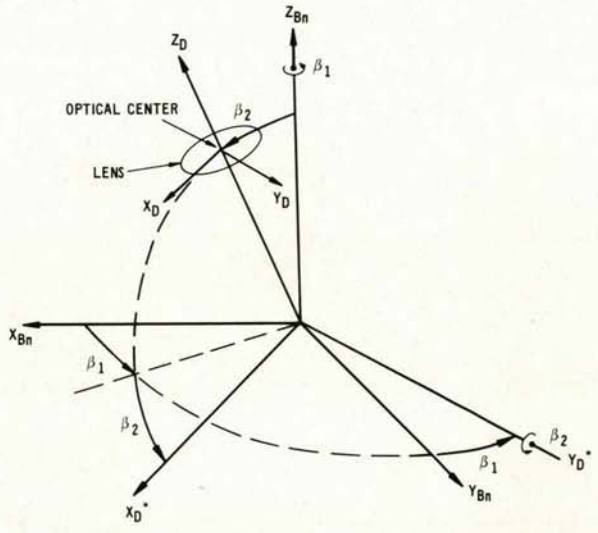

Figure 3. Actual and nominal body fixed reference frames, $\{\bar{X}_B\}$ resp. $\{\bar{X}_{BN}\}$ (sequence of rotations: $\gamma_1 \rightarrow \gamma_2 \rightarrow \gamma_3$; $|\gamma_2|, |\gamma_3| << 1$).

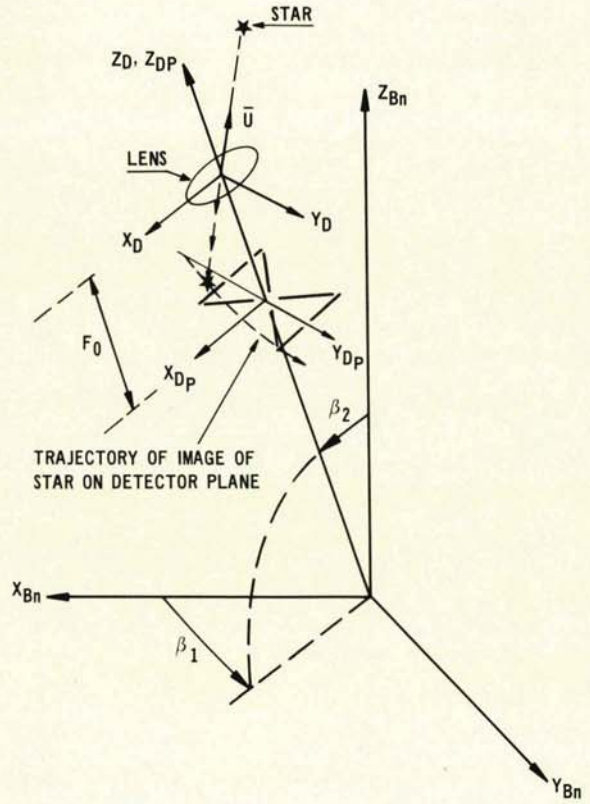

Figure 4. Detector reference frame $\{\bar{X}_D\}$ with origin in optical center; detector plane reference frame $\{\bar{X}_{DP}\}$ parallel, and with origin in detector plane (slit plane).
(F_0 is the focal length of the optics; $\bar{u}$ is the unit vector to star).

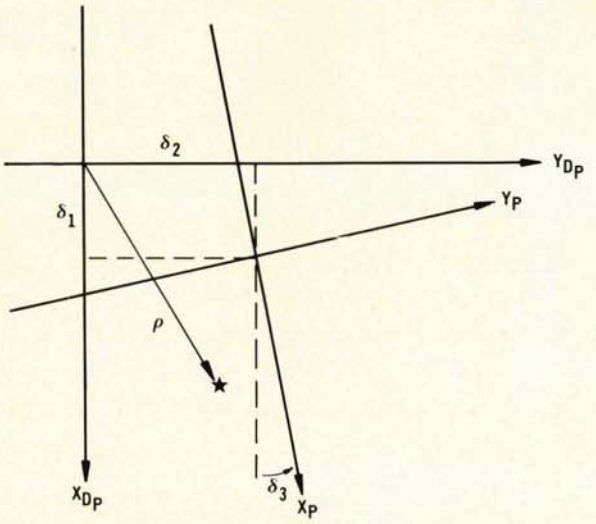

Figure 5. Misalignments $(\delta_1,\delta_2,\delta_3)$ between detector plane reference system $\{\bar{X}_{DP}\}$ and pattern reference frame $\{\bar{X}_P\}$.

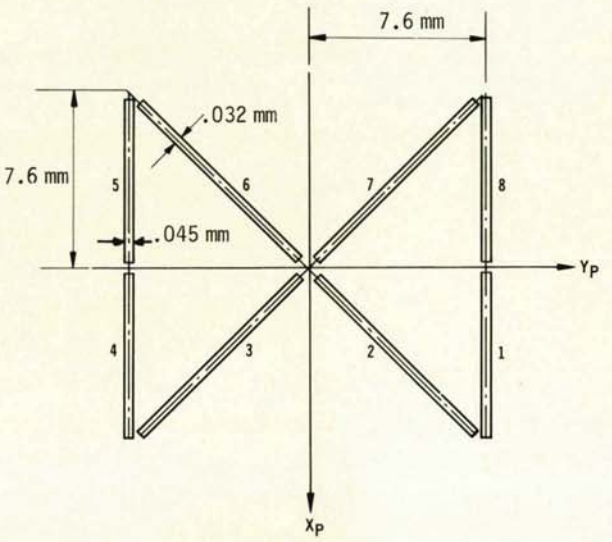

Figure 6. Eight independent ESA starmapper slits in the pattern reference frame $\{\bar{X}_P\}$ (Ref. 5).

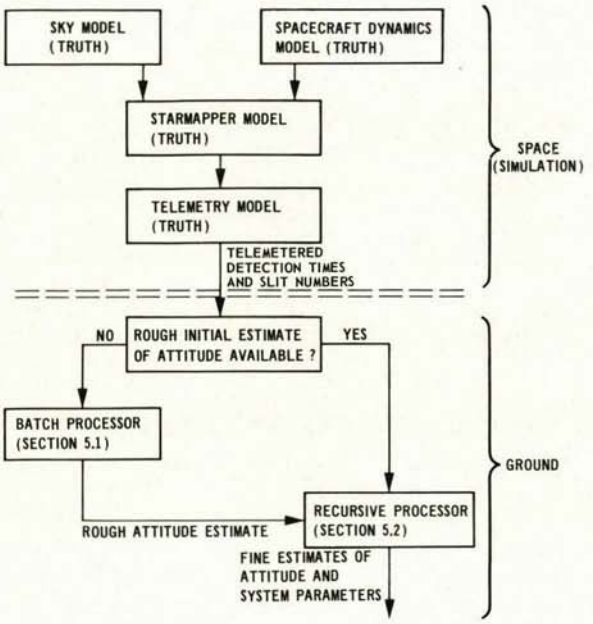

Figure 7. Software developed for end-to-end simulation: truth models to simulate real measurements, and ground-based attitude estimation software (Refs 8-11).

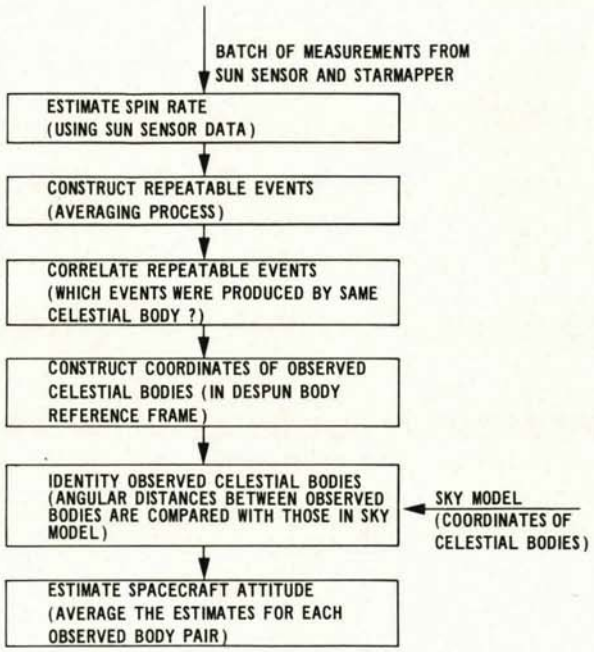

Figure 8. Blockdiagram of the attitude acquisition approach (NLR, Refs 8-9).

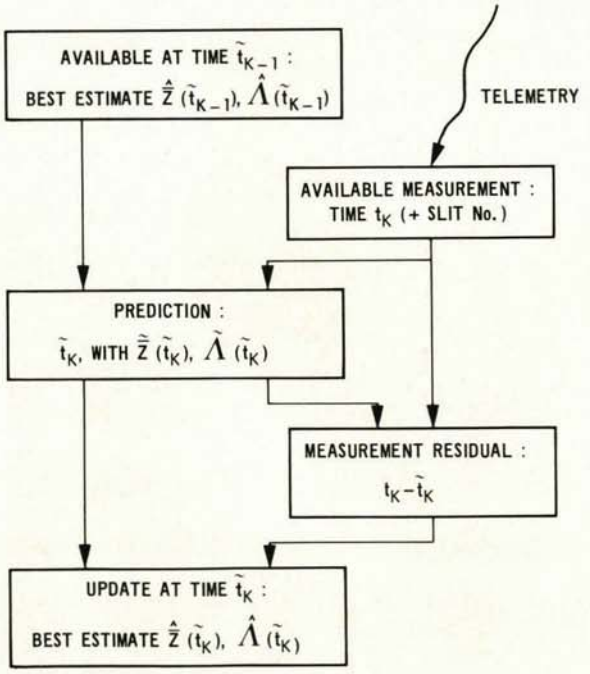

Figure 9. Principle of recursive estimation (NLR, Refs 10-11).

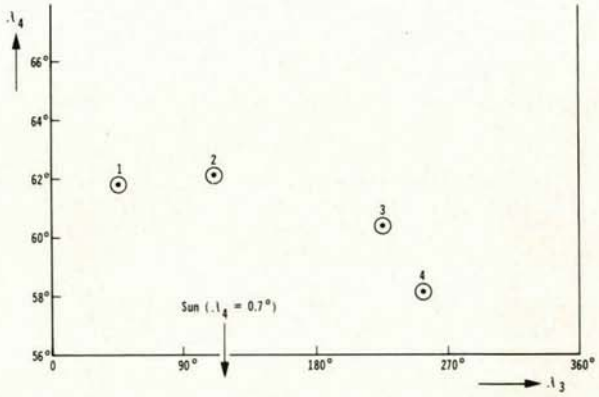

Figure 10. Relative geometry of repeatedly observed and subsequently identified stars (numbers 1-4), and of Sun. (λ_3 = relative azimuth in despun body frame; λ_4 = elevation in despun body frame).

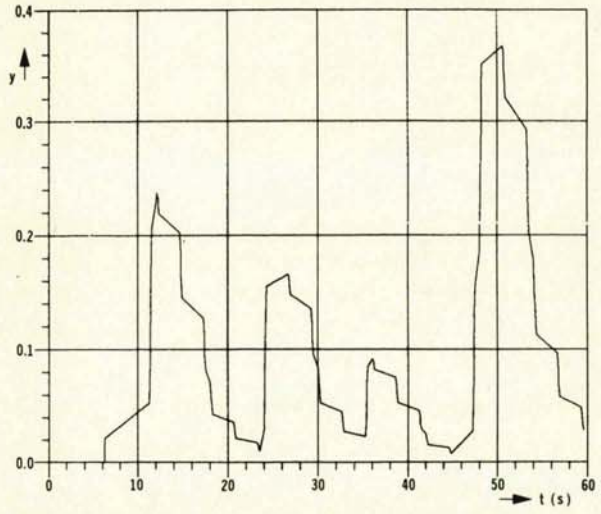

Figure 11. Divergence detection parameter.

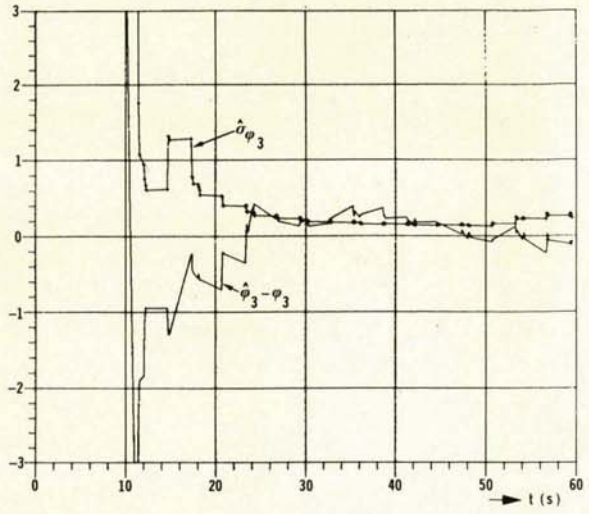

Figure 12. Estimation error and estimated standard deviation of phase angle φ_3 (in arcminutes).

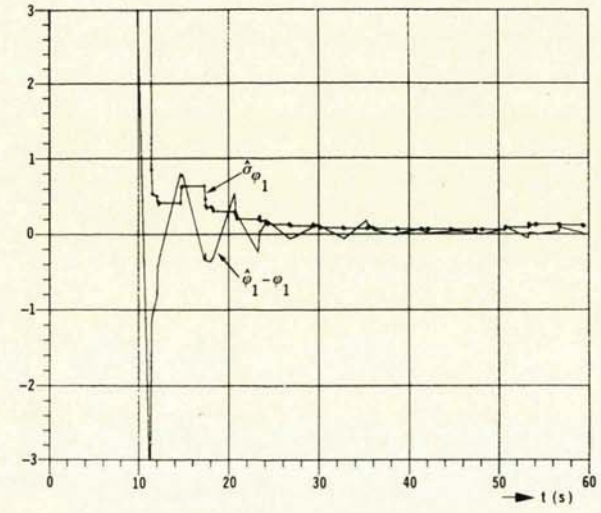

Figure 13. Estimation error and estimated standard deviation in transverse attitude angle φ_1 (in arcminutes).

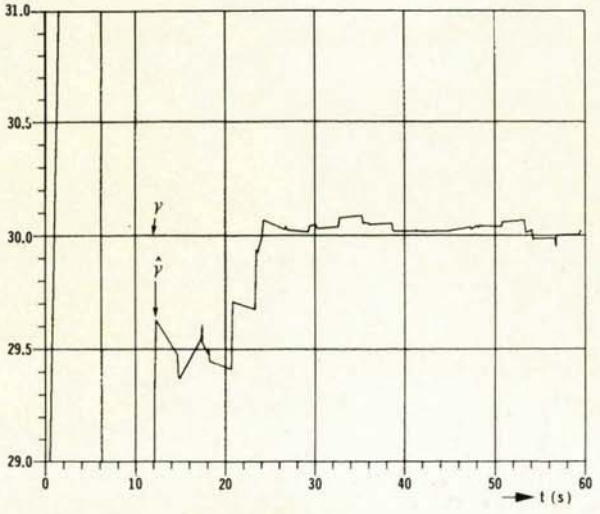

Figure 14. True nutation angle and estimated nutation angle (in arcminutes).

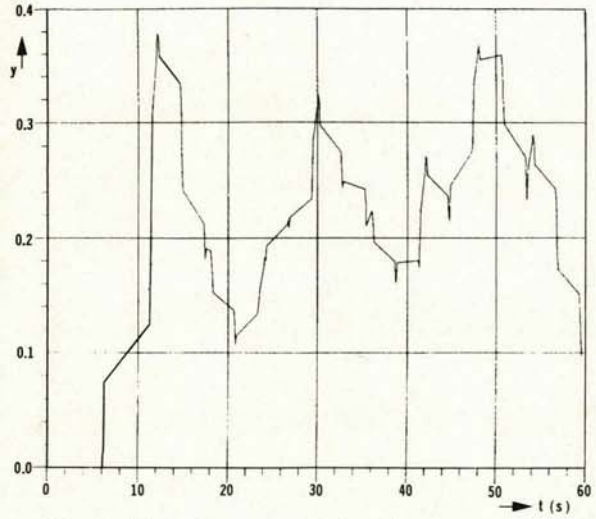

Figure 15. Divergence detection parameter.

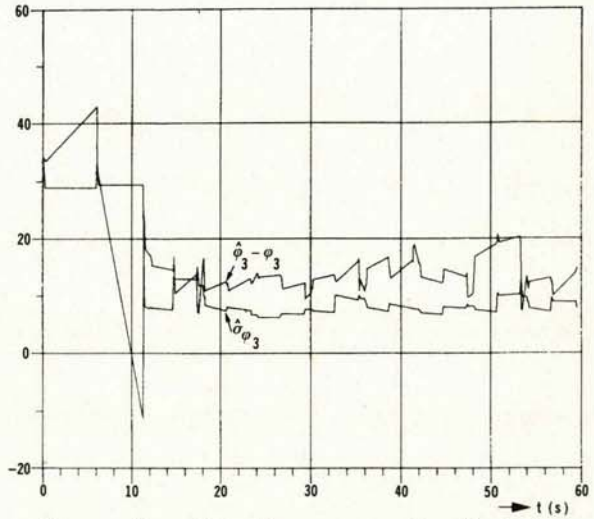

Figure 16. Estimation error and estimated standard deviation of phase angle φ_3 (in arcminutes).

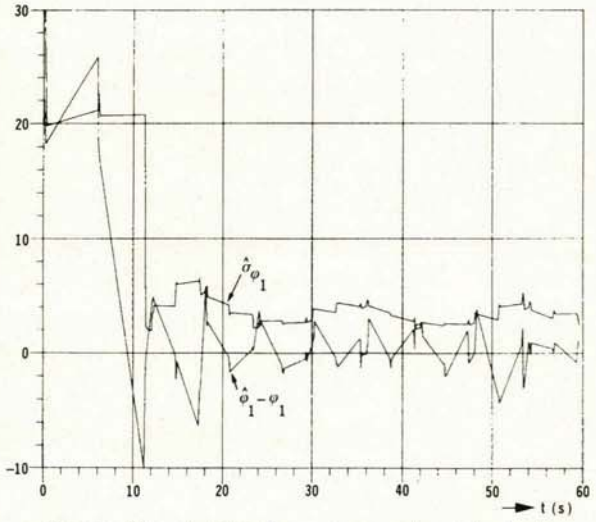

Figure 17. Estimation error and estimated standard deviation in transverse attitude angle φ_1 (in arcminutes).

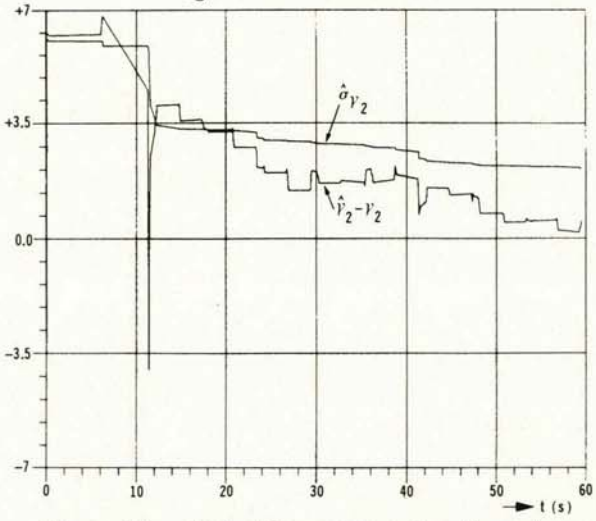

Figure 18. Estimation error and estimated standard deviation in transverse misalignment γ_2 (in arcminutes).

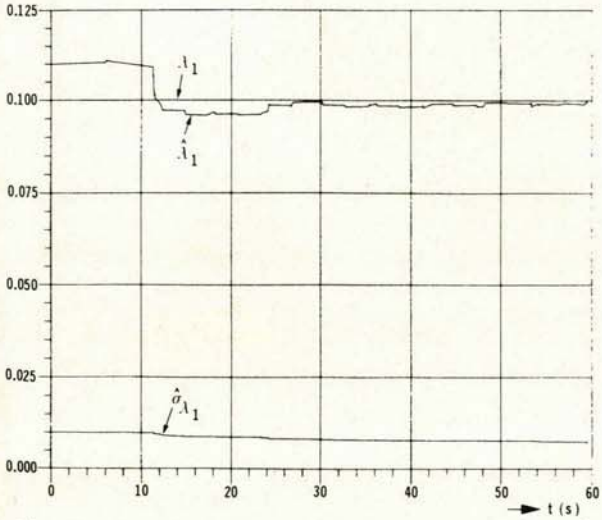

Figure 19. Exact and estimated moment-of-inertia ratio, and estimated standard deviation of estimate (dim. less).

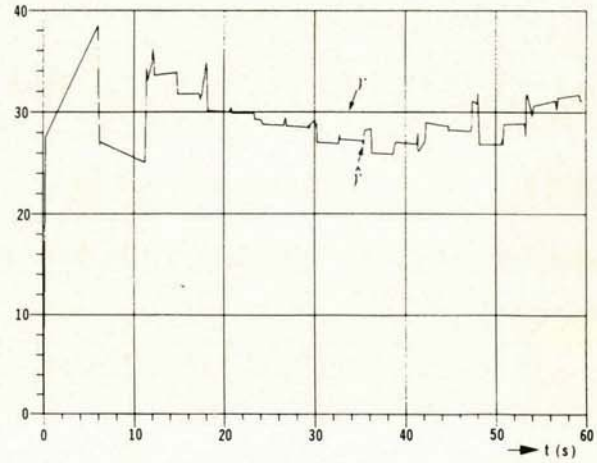

Figure 20. True nutation angle and estimated nutation angle (in arcminutes).